

Gallium- and Cerium-Doped Phosphate Glasses with Antibacterial Properties for Medical Applications

Agata Łapa, Mark Cresswell, Ian Campbell, Phil Jackson, Wolfgang H. Goldmann, Rainer Detsch, and Aldo R. Boccaccini*

Novel cerium- (Ce) and gallium (Ga)-doped phosphate glasses (PGs) are successfully obtained by the peroxidation method. The new glasses are characterized using Fourier-transform infrared spectroscopy (FTIR), Raman spectroscopy, X-ray diffraction, inductively coupled plasma-optical emission spectroscopy (ICP-OES), and pH measurements. A strong correlation between glass properties and their composition is found. The incorporation of Ga/Ce in the glass structure is confirmed by peak shifts in Raman and FTIR spectra. Degradation tests conducted in water confirm the soluble character of the PGs and reveal the influence of Ga and Ce on the degradation rate. Ga-doped glasses are found to be less soluble than Ce-doped ones (43%, 33%, 21%, and 16% of dry mass remained after 7 weeks for 7Ga, 5Ga, 5Ce, and 7Ce, respectively). Biological evaluation using ST-2 cells shows adequate cell response with a cell viability of 80% measured using the indirect contact method depending on the composition. The cell viability decreases with an increase in Ga content and increases with Ce content. The antibacterial character of Ga/Ce-doped PGs is confirmed by turbidity measurements against *Escherichia coli* and *Staphylococcus carnosus*. The novel Ce/Ga-doped PGs exhibiting antibacterial properties and biocompatibility reported here are interesting for tissue engineering and wound healing applications.

$P_2O_5-Na_2O-CaO$)^[1,3–5] comprise elements naturally occurring in the human body.^[6–8] PGs are soluble and their degradation rate can vary from hours to weeks depending on the composition.^[9] The solubility of PGs make them an interesting baseline for controlled delivery of therapeutic or antibacterial ions such as Ag, Cu, or Ga.^[10–15] Moreover, high PG solubility opens up their potential use in soft tissue repair applications (e.g., in contact with skin,^[16] muscle,^[17] and nerve tissues^[18,19]) or as temporary implants dissolving gradually, whilst the healing process takes place.^[20]

The composition of PG strongly influences their potential, in particular the structural, chemical, and biological behavior.^[21–23] For example, an increase in calcium oxide content decreases glass degradation, whereas an increase in P_2O_5 encourages high dissolution rates due to the presence of P–O–P bonds, which lack resistance to hydrolytic attack.^[24]

One of the interesting features of PGs is their ability to release ions known to be antibacterial at controllable rates. The growing problem of antibacterial resistance to antibiotics has pushed scientists to look for alternative solutions.^[25] Each year, the USA spends ≈\$20 billion in treating infections caused by antibiotic-resistant bacteria.^[26] Among the many antibacterial ions available, gallium and cerium show interesting properties.^[27–34] The antibacterial effect provided by gallium is called “the Trojan horse strategy”^[35] as gallium is introduced easily into bacteria due to similarities with iron (Fe). This approach is


1. Introduction

Phosphate glasses (PGs) are promising materials for medical applications due to their controllable solubility in aqueous media. In particular, their ability to continually dissolve can be exploited to release biologically active ions in a controlled, linear manner in applications requiring a biodegradable material in contact with bone and soft tissues.^[1] PGs have lower melting temperatures compared with silicate glasses,^[2] and the most studied compositions (in the system:

Dr. A. Łapa, Dr. R. Detsch, Prof. A. R. Boccaccini
Department of Materials Science and Engineering
Institute of Biomaterials
University of Erlangen-Nuremberg
Cauerstraße 6, 91058 Erlangen, Germany
E-mail: aldo.boccaccini@fau.de

Dr. A. Łapa, Dr. M. Cresswell, I. Campbell, Dr. P. Jackson
Lucideon Ltd UK
Queens Road, Stoke on Trent ST4 7LQ, UK

Prof. W. H. Goldmann
Department of Biophysics
University of Erlangen-Nuremberg
Henkestraße 91, 91052 Erlangen, Germany

 The ORCID identification number(s) for the author(s) of this article can be found under <https://doi.org/10.1002/adem.201901577>.

© 2020 The Authors. Published by WILEY-VCH Verlag GmbH & Co. KGaA, Weinheim. This is an open access article under the terms of the Creative Commons Attribution-NonCommercial License, which permits use, distribution and reproduction in any medium, provided the original work is properly cited and is not used for commercial purposes.

DOI: 10.1002/adem.201901577

a nonspecific and effective way of inducing metabolic distress in fast-growing cells such as bacteria.^[30] Fe(III) is an important element that almost all bacteria require for their growing process, whereas Ga has an almost identical ionic radius, coordination chemistry, and ionization potential to Fe(III); thus, it can be actively transported into bacteria but it cannot be used in any metabolic pathways.^[30] Moreover, gallium is important in bone modeling, supporting hydroxyapatite formation,^[36] and is used to accelerate bone resorption.^[37]

Gallium-doped glasses have been extensively studied in recent years, showing antibacterial effectiveness and cytocompatibility.^[38] Pourshahrestani et al.^[39] reported 3 mol% Ga₂O₃ mesoporous bioactive glasses to be more effective against *Staphylococcus aureus* than equivalent 1 and 2 mol% doped glasses. In studies by Sanchez-Salcedo et al.,^[40] 5 mol% Ga₂O₃ containing silicate bioactive glasses showed antibacterial properties against *S. aureus* and *Pseudomonas aeruginosa*. Gómez-Cerezo et al.^[41] investigated the biological effect of Ga on osteoblasts and osteoclasts, showing selective behavior toward different cell types (Ga-mesoporous bioactive glass simulates early differentiation of preosteoblast while disturbing osteoclastogenesis).

Cerium oxide (ceria, CeO₂), which is also known to be antibacterial, has antioxidant properties. The antimicrobial mechanism can be explained as an ability to dissociate the outer membrane of bacterial cells from their cytoplasmic membrane.^[33] Moreover, Ce ions are used for the treatment of severe burns^[33] and nanoparticles of cerium oxide have been proven to support fibroblast, keratinocyte, and vascular endothelial cell growth.^[42] Zhang and co-workers^[43] showed the positive effect of cerium oxide on proliferation, differentiation, and mineralization of primary osteoblasts. Studies on silicate bioactive glasses doped with Ce have shown noncytotoxicity, and good cell attachment, with cells well spread on the glass surface.^[34] Interest in the application of cerium has grown due to its antioxidant properties linked to nerve regeneration and reconstruction. The high field strength of cerium creates strong covalent bonding which leads to a decrease in glass dissolution and associated release of Ce⁴⁺/Ce³⁺.^[44] Moreover, both Ce and Ga are multivalent ions which, in contrast to monovalent Ag, strengthen the glass network by increasing connectivity to P—O— groups.^[45–49]

The aim of the current study was to investigate both the biological and antibacterial ability of gallium- and cerium-doped PG and to determine how these elements influence the PG structure and behavior. To achieve a balance between strong antibacterial capability provided by Ga and therapeutic properties provided by Ce, a dual doped PG has been proposed anticipating that coaddition of Ga and Ce will enable to study possible synergistic effects in this novel PG.

2. Experimental Section

2.1. Materials

The following powder precursors were used: calcium carbonate (Sigma Aldrich, ≥99.0%), sodium phosphate monobasic (Sigma Aldrich, ≥99.0%), magnesium phosphate dibasic trihydrate (≥98.0%), monoammonium phosphate (Sigma Aldrich,

≥98.0%), gallium oxide (Sigma Aldrich, ≥99.99%), and cerium dioxide (Sigma Aldrich, ≥99.99%).

2.2. Preparation of PG

Seven new glasses (Table 1) were melted using peroxidation as an extra step during the manufacturing process (Figure 1). This was applied due to the concerns over intense vaporization of the glass precursors. The powder precursors defined in Section 2.1 were mixed, sieved (aperture diameter of ≈2 mm), and placed inside an alumina crucible. The crucible was placed inside the furnace and heated for 1 h at 200 °C and then 1 h at 700 °C. Premelted glass was carefully (manually) removed from the inner side of a crucible (to avoid alumina contamination) and placed in a platinum crucible inside a preheated kiln (at 1150 °C). After 1.5 h, the glass melt was poured onto a metallic plate. The glass frit was milled down into powder (<150 μm) using a planetary ball mill (Fritsch, Planetary Micro Mill Pulverisette 7) for the next experiments.

2.3. X-Ray Diffraction Analysis

Glass powder samples were characterized by X-ray diffraction (XRD) using a MiniFlex600 diffractometer (Rigaku, Japan). The samples were continuously spun during data collection and scanned over a 2θ range of 20–80° with a 0.02° step^{−1} at 4° min^{−1}.

2.4. Fourier-Transform Infrared Spectroscopy

The chemical structure of the powder samples was analyzed using a Fourier-transform infrared (FTIR) spectrometer (IRAffinity-1S, SHIMADZU, Japan). Each powder glass sample spectrum was acquired and averaged with a resolution of 4 cm^{−1}, over scans 20–40 and a range between 400 and 4000 cm^{−1}. The peak wavenumbers were labeled using Origin 9.0 (OriginLab, USA) software.

2.5. Raman Spectroscopy

Raman spectroscopy was performed using a HeNe laser Spectrum (Jobin Yvon Horiba) and an optical microscope (Olympus, Japan) and analyzed using LabSpec (Horiba). The glass samples in powder form were characterized in the

Table 1. PGs—list of developed compositions.

Glass	Composition [mol%]						Melting temperature [°C]
	P ₂ O ₅	MgO	CaO	Na ₂ O	Ga ₂ O ₃	CeO ₂	
5Ga	45	25	15	10	5	—	1150
5Ce	45	25	15	10	—	5	1150
7Ga	45	24	14	10	7	—	1150
7Ce	45	24	14	10	—	7	1150
3Ga2Ce	45	25	15	10	3	2	1150
45P	45	25	20	10	—	—	1150

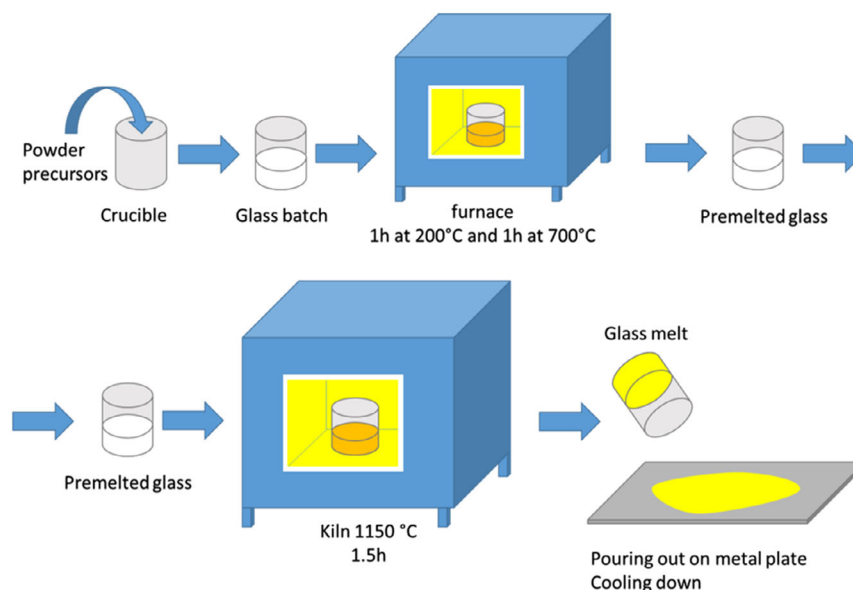


Figure 1. Schematic representation of the peroxidation method, an alternative way of obtaining PGs.

wavenumber range of $400\text{--}1400\text{ cm}^{-1}$ with an acquisition time of 30 or 15 s, depending on the sample.

2.6. Degradation Test of PG

Dissolution tests were performed by placing 0.4 g of powder sample (three replicas) into glass bottles with 40 mL of deionized water. Samples were incubated at 37°C under dynamic conditions (shaking at 125 rpm). Every 7 days, the samples were filtered (to remove water), washed with deionized water, and dried in an oven (at 37°C overnight). After weighing, the samples were placed back in deionized water for further investigation. The dry mass of samples was measured using a laboratory balance (Ohaus Analytical Plus, NJ, USA).

Percentage of dry mass was determined according to Equation (1)

$$\%_{\text{dried mass}} = \frac{m_{\text{dried}}}{0.4} \times 100\% \quad (1)$$

where m_{dried} is the mass of a sample after drying (in grams) and 0.4 is the mass of the initial sample (in grams).

2.7. pH Measurements

The pH of samples were measured using a HANA pH meter during incubation in deionized water under dynamic conditions at 37°C .

2.8. Inductively Coupled Plasma-Optical Emission Spectroscopy

Inductively coupled plasma-optical emission spectroscopy (ICP-OES) analysis of glass powder samples (1 wt/vol%) incubated at 37°C in cell culture medium [CCM, containing RPMI (Roswell Park Memorial Institute) + 10 vol% fetal bovine

serum, +1 vol% penicillin streptomycin solution, Gibco, Sigma Aldrich, Germany] was conducted predominantly using helium as the collision gas to remove polyatomic (oxide-based) mass interferences by kinetic energy discrimination (KED). In some cases, such as for calcium determination, analyses were also conducted using hydrogen reaction gas to remove doubly charged mass interferences by charge transfer. The raw counts for each analytical mass were translated to a concentration by the Agilent MassHunter software after a multipoint calibration with linear fit ($r^2 > 0.999$). Over-range samples were diluted in a 2% nitric acid matrix to match the calibration standards.

2.9. Viability Assay of ST-2 Cells in Indirect Contact with PG

2.9.1. Set Up

Glasses 45P, 5Ga, 7Ga, 2Ga3Ce, 5Ce, and 7Ce were tested using bone marrow stromal cells (ST-2, Deutsche Sammlung für Mikroorganismen und Zellkultur, Germany) isolated from the bone marrow of BC8 mice, by an indirect method, described by Balasubramanian et al.^[50] Glass powders were sterilized using the dry heating method for 2 h at 160°C . Of each glass sample, 0.1 g was incubated in 10 mL of CCM for 24 h at 37°C . The CCM uses RPMI medium (1640, 1×, Gibco by Life Technologies, Germany) containing 10 vol% of fetal bovine serum (Sigma Aldrich, Germany) and 1 vol% penicillin streptomycin solution (Sigma Aldrich, Germany). Of $100\,000\text{ cells mL}^{-1}$, 1 mL was seeded in every well of a 24-well plate and incubated over 24 h. Once the cells had attached to the polystyrene well surface, the medium was removed and replaced with supernatant from the preincubated glass powder. ST-2 cells were incubated for another 48 h (Figure 2).

To measure cell activity and morphology, WST-8 test^[51] and histochemical staining for hematoxylin and eosin (H&E)^[52] (HE kit, Sigma Aldrich, Germany) were applied. The cell viability

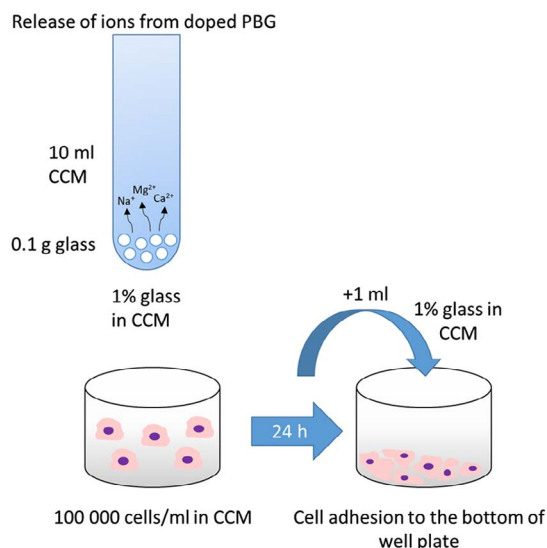


Figure 2. Cell viability study setup. The glass powder is incubated in CCM for 24 h, inducing release of ions, later the ST-2 cells are incubated for 48 h in medium containing the glass dissolution products.

was measured by the conversion of tetrazolium (WST-8, Sigma) to formazan by intracellular enzymes.

2.9.2. WST-8 Assay

After 48 h of incubation, the medium was removed and replaced with 0.5 mL of 1 vol% solution of WST-8 in CCM. Again, samples were incubated at 37 °C for 2 h until the medium changed color. After that, 100 μ L of solution from each well were transferred into a 96-well plate, and the absorbance at 450 nm was measured using a microplate reader PHOmo (Anthos, Germany). The results were subtracted from the blank (1 vol% WST-8 solution in CCM) and compared with the positive control: standard cell culture of ST-2 cells. All results were expressed as mean \pm standard deviation. Significant differences have been statistically assessed using one-way ANOVA to compare multiple datasets ($p < 0.05$).

2.9.3. H&E Staining

To investigate the morphology of the cells, H&E staining was applied. First, all cells were washed with double phosphate-buffered saline (DPBS; Gibco by Life Technologies, Germany) solution and fixed to the bottom of well plates using the fixing solution Fluofix containing 4 vol% formalin. Fluofix was removed after 15 min, and all wells were washed with distilled water. Next, hematoxylin was added to every well for 15–20 min to stain the cell nucleus. Again, samples were washed with water and Scott's tap water ($\text{MgSO}_4 \cdot 7\text{H}_2\text{O}$, 200 g L^{-1} + NaHCO_3 , 20 g L^{-1} , Sigma Aldrich, Germany) was added to change the pH. After 5 min, the washing process was repeated, and eosin solution was added for 1–5 min to stain the cytoplasm. The eosin solution contained 0.4 vol% of eosin in 60 vol% ethanol and 5 vol% acetic acid. In the last step, all wells were first washed with 95 vol% ethanol and later with 100% of ethanol, and were left overnight

to dry. Such samples were ready for imaging using a light microscope (AxioVert Zeiss, Germany).

2.10. Antibacterial Evaluation

Both colonies, *Escherichia coli* (gram-negative) and *Staphylococcus carnosus* (gram-positive), were moved and incubated separately in 10 mL of Luria/Miller medium (LB medium; Carl Roth, Germany) for 24 h at 37 °C. After 24 h, the necessary volume (in microliter) of bacteria broth was added to 1 mL of bacteria-free medium to achieve a measured optical density (OD) equal to 0.015 at a wavelength of 600 nm in the photometer. To a 24-well plate, 0.1 g of each glass powder was added followed by 2 mL of medium to obtain a concentration of 5%. Later, bacteria broth was added, generating an OD of 0.015 for each sample.^[53] Similar well plates were prepared for both gram-positive and gram-negative bacteria and incubated for 48 h. The OD of each sample (three replicas) was measured after 4, 24, and 48 h.

3. Results and Discussion

3.1. XRD

XRD data confirmed the amorphous character of the glasses (Figure 3). No peaks indicating crystalline phases were detected for any of the samples. The results are similar to the XRD spectra reported for other PGs.^[54]

3.2. FTIR

The FTIR spectra for the PGs investigated (Figure 4) show the presence of peaks that are characteristic of glasses with 45 mol% P_2O_5 . Q^1 and Q^2 units can be identified, with details including their corresponding peak positions shown in Table 2. Peaks in the range of 731–750 cm^{-1} are attributed to symmetric stretching of P–O–P in Q^1 units, whereas peaks around 900 cm^{-1} (895–910 cm^{-1}) are known to be asymmetric stretching vibrations of Q^2 .^[55] Peaks observed at 1000 cm^{-1} are the vibrations of terminal groups P–O $^-$ in Q^1 and arise due to the action of modifier oxides on the glass network.^[55]

For gallium-doped glasses, the first peak ($\approx 478 \text{ cm}^{-1}$) is clearly shifted. Interestingly, all Ga-doped glasses (5Ga, 7Ga, and 2Ga3Ce) do not show a fifth peak around 1250 cm^{-1} , which is characteristic for ν_{as} (asymmetric stretching) of two nonbridging oxygens bonded to the P atom in a Q^2 . Similar behavior was reported for Ga-doped PGs by Stuart et al.^[47] This behavior has been attributed to a reduction in Q^2 species and a more depolymerized glass network structure.^[47] Higher vibrational frequencies of peaks around 1100 cm^{-1} for glasses 7Ga and 7Ce suggest greater packing density.^[47] Moreover, the intensity of these peaks increases with an increase in dopant level.^[56] Glasses doped with Ga show shifts of peaks around 900 cm^{-1} into a higher wavenumber range with increasing gallium content, whereas the same peak does not change its position with an increase in Ce content. However, the intensity of these peaks increases suggesting high asymmetric stretching modes of P–O–P.

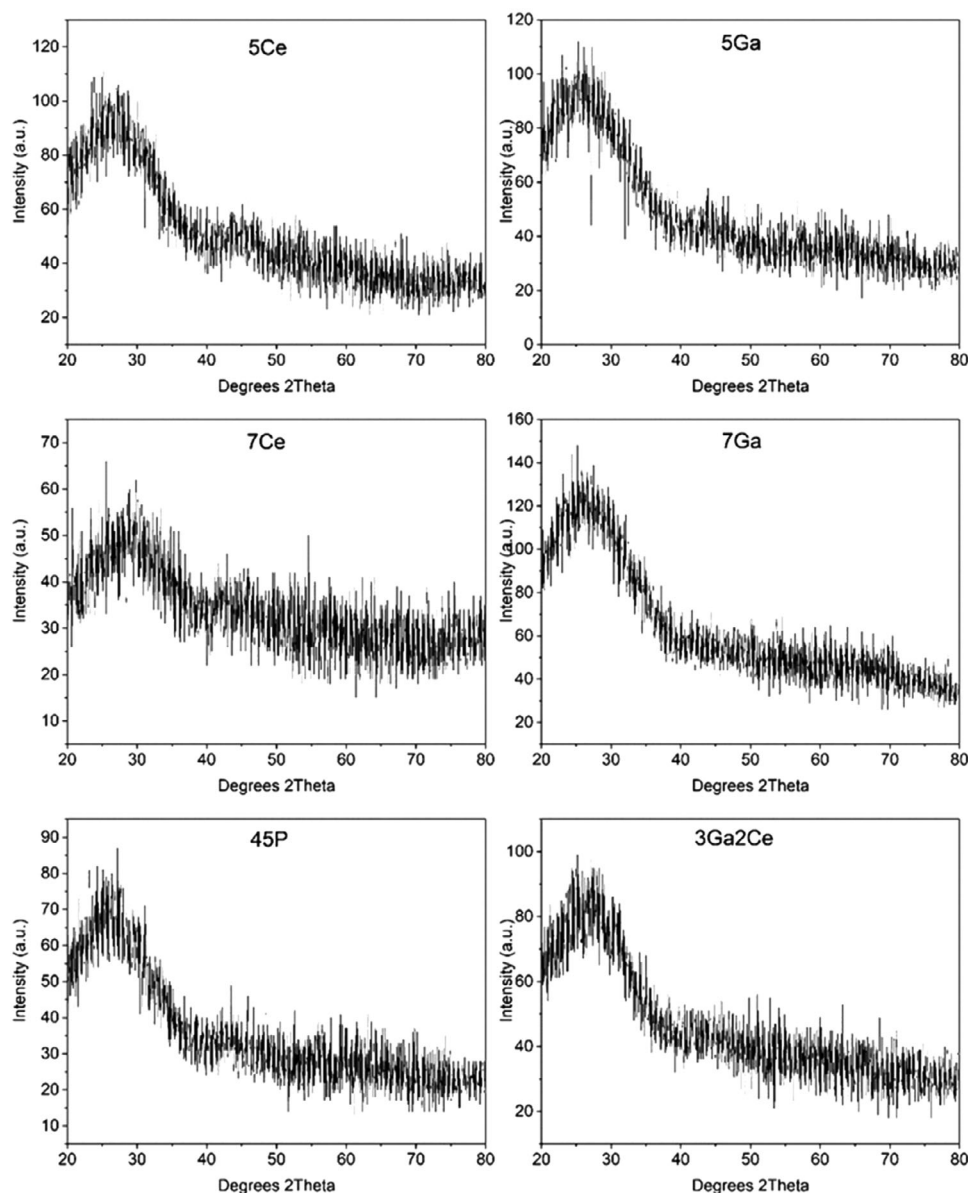


Figure 3. XRD spectra for doped PG incorporating Ga/Ce confirming the amorphous character of all investigated glasses.

3.3. Raman Spectroscopy

Raman spectra for PGs doped with cerium and gallium (shown in **Figure 5** and **Table 3**) display all the characteristic peaks for Q^1 and Q^2 . The Raman spectra for basic PG consist of peaks at 1380, 1260, 1170, 960, 690, and 620 cm^{-1} . These peaks can be assigned to symmetric stretching vibration of P–O, symmetric stretching of P–O, symmetric stretching of a nonbridging oxygen on a Q^2 , symmetric stretching of the orthophosphate groups PO_4^{3-} , and symmetric vibration of P–O–P, respectively.^[57] All of these peaks (as well as additional peaks) were present in the analyzed samples. The peak near 425 cm^{-1} corresponds to the O–P–O bending mode. The 510 cm^{-1} peak is a bending vibration of P–O bonds, and peaks near 1090 cm^{-1} are characteristics of

PO_2 symmetric stretching of non-bridging oxygen on Q^1 units.^[57] Peaks near 880 cm^{-1} (877–895 cm^{-1}) could be interpreted as asymmetric stretching of P–O–P.^[57] Slight shifts between peaks do not follow any obvious trends.

The intensity of the two peaks at 710 and 1100 cm^{-1} increases with rising dopant levels. Moreover, a double peak at 1100 cm^{-1} can be observed. Lower noise can be seen for spectrum 5Ga, where peaks are symmetrical, and the peak at 450–650 cm^{-1} is much flatter than in the spectra of other glasses. Glasses 45P, 7Ga, 7Ce, 5Ga, and 3Ga2Ce have strong overlapping double peaks around 1000 cm^{-1} , and the peaks are much sharper.

The peaks at 1250 cm^{-1} increase to higher wavenumbers with a rise in the dopant content. The bonds are cation-dependent and the frequency values increase with an increase in the

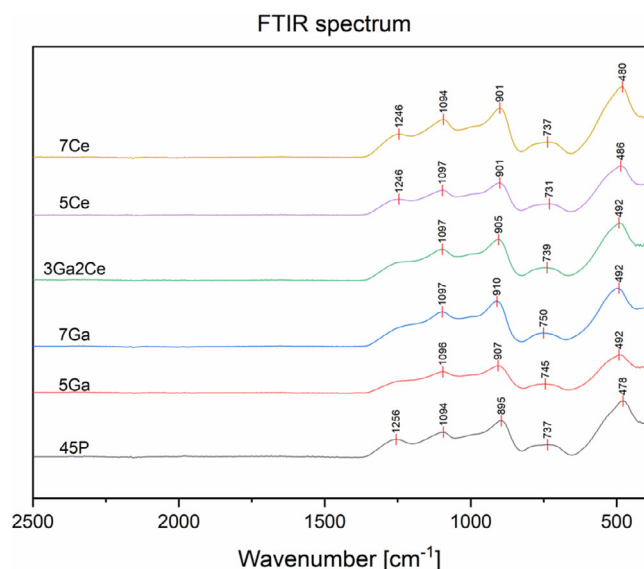


Figure 4. FTIR spectra for doped PGs, the relevant peaks are shown in Table 2.

electronegativity of the dopants (Ga 1.84, Ce 1.12).^[61] The wavenumber of the peaks suggests the presence of strained P—O—P bonds. The peaks around 860 and 980 cm^{-1} are more intense for glasses 7Ga and 3Ga2Ce, this suggests a decrease in the strength of the covalent bond P—O when phosphorous is replaced with another ion.^[57]

3.4. Degradation Test

Dissolution rates for all glasses were found to be uniform and decreased with time (Figure 6). The weight loss of PGs follows two kinetic phenomena: 1) as a function of $t^{1/2}$ or 2) linear with t (where t represents time).^[62] Undoped glasses (45P) dissolved completely after 7 weeks with around 50% of dry mass remaining after 3 weeks. The results are in agreement with the literature where a low content of sodium (10 mol%)^[63] or high content of magnesium (25 mol%)^[54] and calcium^[63] have been reported to decrease the dissolution rate of PG. Na^+ as a monovalent ion depolymerizes P—O—P chains and creates nonbridging oxygens, which disturb the glass network.^[63] A similar effect can be

observed for Ca^{2+} , however due to its charge, calcium still forms connective bonds with two oxygens, which results in a stronger network.^[63] Addition of Ga and Ce tends to decrease dissolution rate with 45% of dry mass remaining after 7 weeks of incubation for glasses doped with 7 mol% of Ga. After 5 weeks the dissolution rate for the glass with 5 mol% Ga is lower than that of glasses doped with 7 mol%.

The decrease in degradation of P_2O_5 —CaO— Na_2O glass with an increase in Ga content is in agreement with studies by Valappil et al.^[14] Gallium oxide stabilizes the glass structure and can play a role as both glass modifier and glass former when the amount of Ga is high, or phosphate chains are short.^[64] Moreover, Ga—O bonds have a covalent character,^[64] and they increase network connectivity^[65] creating relatively strong covalent Ga—O—P bonds when Ga enters the glass-forming phosphate chain network. In addition, the presence of Ga can lead to the formation of Ga—O—Ga bonds that can stabilize the glass structure and increase durability.^[66]

Interestingly, higher amounts of cerium oxide slightly decrease dissolution rates of PG (5 and 7 mol%). Cerium oxide acts as a glass modifier.^[56] Incorporation of Ce into a PG network causes an increase in the glass cross-linking density and chemical durability.^[56] Only nominal decreases in degradation kinetics due to increased levels of Ce could suggest an optimal level of cerium oxide, beyond which it does not disturb the PG structure. Cerium oxide can exist in two oxidation states in the glass network, namely as Ce^{4+} or/and Ce^{3+} .^[67] Literature report differences in the glass structure as Ce^{4+} have higher field strength, shorter Ce—O bonds, and lower coordination number than Ce^{3+} , allowing the creation of stronger bonds.^[67] Increase in Ce^{3+} over Ce^{4+} causes a weakening in the binding effect of bridging oxygens and the strengthening of nonbridging oxygens.^[68] However, the overall impact of Ce addition on the dissolution rate of PG is not conclusive. According to the literature, introduction of cerium ions can increase the amount of Q^2 , making the glass more hydrolytically resistant versus nondoped compositions (that contains Q^3 units), due to the formation of strong P—O chains with P—OH hydrogen bonds.^[69] In contrast, Lai et al.^[45] reported that increases in Ce content leads to an increase in Q^2 species and an increase in Tg as a result of shorter and stiffer Q^2 chains. It is likely that shorter phosphate chains are hydrated and solubilize much quicker than longer phosphate chains, which could explain the enhanced dissolution rate. In addition, a decrease in Q^1 and increase in Q^2 is accompanied

Table 2. Identification of the FTIR peaks of doped PG.

Value wavelength [cm^{-1}]						Interpretation
45P	5Ga	7Ga	2Ga3Ce	5Ce	7Ce	
478	492	492	492	486	480	May attribute to the deformation modes of phosphate tetrahedral and vibration of cation oxygen polyhedron ^[45]
737	745	750	739	731	737	Symmetric stretching mode of the nonbridging oxygen stretching modes vibrations bonds Q^1 species ^[45]
895	907	910	905	901	901	Symmetric stretching vibration of P—O—P linkages in Q^2 ^[45]
1094	1096	1097	1097	1097	1094	Asymmetric stretching mode of the nonbridging oxygen stretching modes vibrations bonds Q^1 species ^[45]
1256	—	—	—	1246	1246	Asymmetric stretching vibration of P—O—P linkages in Q^2 species ^[45]

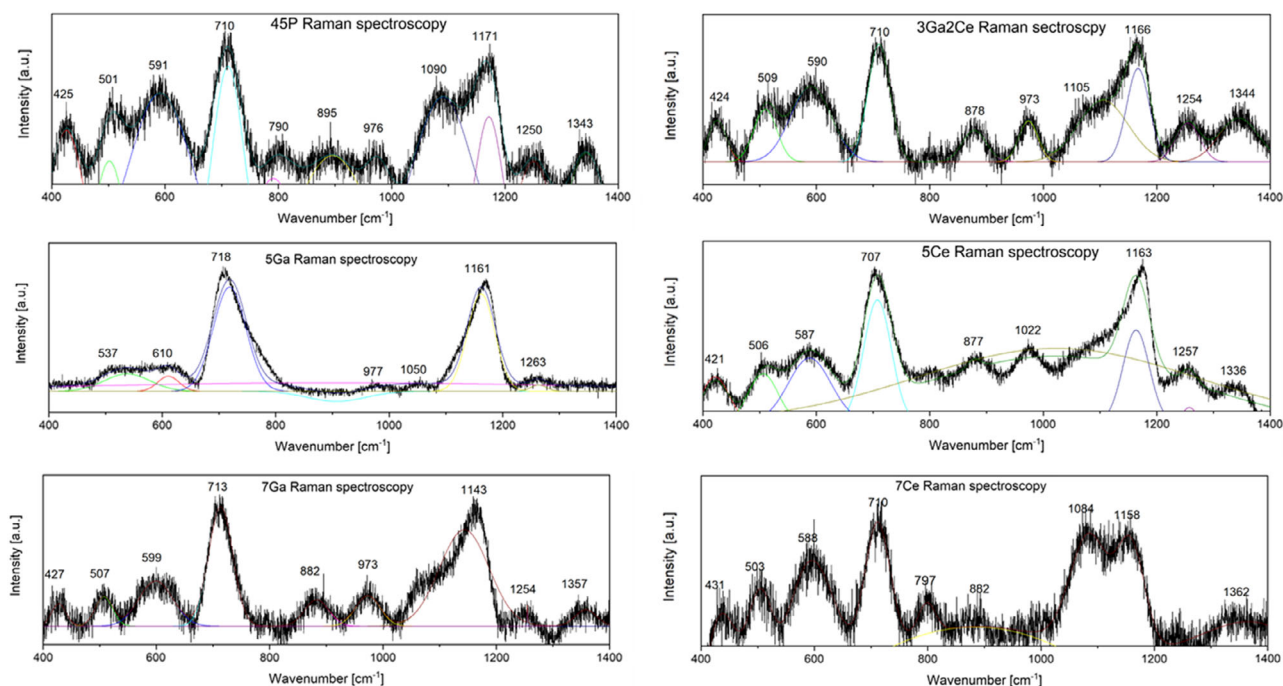


Figure 5. Raman spectra of doped PGs (45P, 5Ga, 7Ga, 3Ga₂Ce, 5Ce, 7Ce). The characteristic peaks are shown in Table 3.

Table 3. Raman spectroscopy of doped PGs (45P, 5Ga, 7Ga, 3Ga₂Ce, 5Ce, 7Ce).

Value wavenumber [cm ⁻¹]						Interpretation of the peaks
45P	5Ga	7Ga	3Ga ₂ Ce	5Ce	7Ce	
425	–	427	424	421	431	The P–O bond bending mode of Q ² and Q ¹ units ^[57]
501	537	507	509	506	503	Bending vibration of P–O bonds ^[57]
591	610	599	590	587	588	500–625 cm ⁻¹ region has been attributed to the bending vibrations of the P–O bonds and in chain P–O–P stretching vibrations
710	718	713	710	707	710	P–O–P chains ^[58] symmetric stretching mode in Q ¹ and Q ²
790	–	–	–	–	797	747 cm ⁻¹ , which is assigned to the symmetric stretching mode of P–O–P bridging bond in Q ¹ structure ^[45]
895	–	882	878	877	882	Near 900 cm ⁻¹ symmetric stretching of P–O–p ^[57]
976	977	973	973	–	–	Terminal PO ₃ ²⁻ symmetric groups in Q ¹ pyrophosphates ^[57]
1090	–	–	1105	–	1084	Symmetric stretching vibration of PO ₃ groups ^[57]
–	1050	–	–	1022	–	Near 1050 cm ⁻¹ symmetric stretching vibration of diphosphates in Q ¹ unit ^[59]
1171	1161	1143	1166	1163	1158	Symmetric nonbridging oxygens in Q ² ^[60]
1250	1263	1254	1254	1257	–	Symmetric stretching of P–O ^[57]
1343	–	1357	1344	1336	1362	P=O of terminal oxygen ^[58]

by the formation of Q⁰ ($2Q^1 \leftrightarrow Q^2 + Q^0$ ^[45]), and this effect could possibly explain the increase in dissolution rate. Indeed, the FTIR spectrum of glass 7Ce shows intensive peaks at 900 and 1246 cm⁻¹, which are characteristics of Q² units.

Structural analysis was not pursued further because of a research focus on PG contribution to biological and antibacterial properties. However, further studies (NMR, X-ray photoelectron spectroscopy [XPS], and so on) will be required to fully confirm the detailed glass structure of the ion-doped PGs defined in this article.

3.5. pH Measurements

Measurements were conducted over 7 days and all PG showed a general trend toward decreased pH values as function of time (Figure 7). PG with cross-linked chains tend to decrease the pH of the surrounding solution more readily.^[70] The reduction of pH due to PG dissolution has been associated with degradation of the glass structure and the associated release of phosphate chains, which can form an aqueous solution of phosphoric acids.^[17] The pH drop resulting from dissolution of doped PG

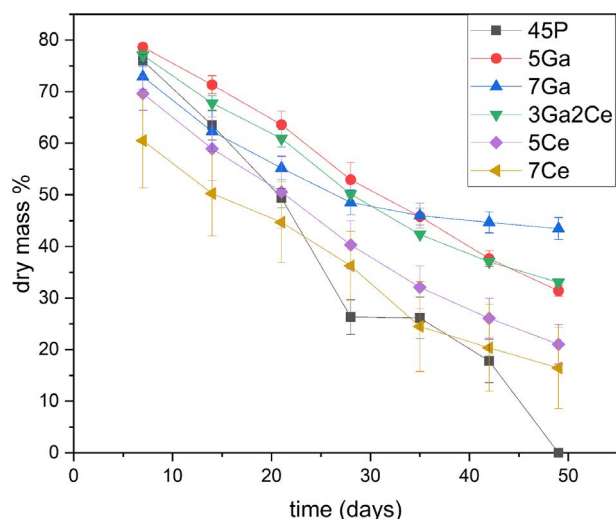


Figure 6. Dissolution of PG in deionized water decreases with time, addition of gallium and cerium decreases dissolution rate, in comparison with undoped glasses; however, the gallium has a higher impact on the glass stability in water.

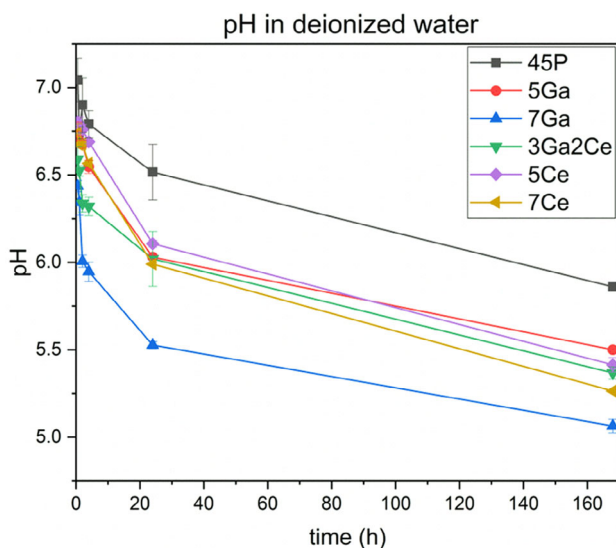


Figure 7. Results of pH measurements in deionized water during 7 days of incubation: in all PG, pH decreases with time.

is seen to be strongly influenced by dopants and decreases as a function of time with the lowest value measured for 7Ga after 7 days. This is in agreement with the acidic/alkali character of the elements based in turn on their position in the periodic table (cerium is less acidic than gallium). Studies on gallium- and cerium-doped borate glasses have also shown a decrease in pH with an increase in Ga/Ce content.^[65] Moreover, in studies by Valappil et al.,^[14] the pH of Ga-doped PG decreased from 8.5 to neutral with increasing Ga content (0–5 mol%). The decrease in pH agrees with previous studies on several PG and PG fibers (PGF).^[71] Interestingly, even if the addition of Ga reduces glass solubility, the pH change of Ga containing PG is consistently

found to be more significant than that of Ga-free PG (45P). This marked reduction in pH could be related to the significant leaching of Ga ions from the glass, according to ICP measurements, as discussed later.

3.6. ICP-OES

The ICP results indicate the release of ions from the glass into the CCM after 24 h of incubation. The presented values (**Figure 8**) correspond to the composition of the medium added to the cells during all performed and described tests. Interestingly, the release of gallium ions for sample 7Ga (24.6 mg L⁻¹) is high, which could be an effect of the interaction with amino acids present in the medium; an accelerated release of ions in CCM was described by Hansen and Thünemann (although for silver nanoparticles).^[72] This could be the case for Ga³⁺, although the formation of GaCl₃ due to a high amount of chloride ions might also be a contributory factor. Moreover, CCM is indeed more complex^[73] than deionized water rendering it capable of changing the balance and preferable dissolution of the ions.^[74] Another important factor is the pH. The pH of deionized water becomes acidic during dissolution studies, whereas CCM has neutral to basic pH. Interestingly, the ICP results show an increase in release of P ions (glasses 5Ce and 7Ce), which may explain the decrease in pH. The release of ions from a soluble system such as PG may raise concerns about the cytotoxicity of the ions. Studies on nerve line cells (HT22) and mouse macrophages (RAW164) have shown toxicity for 20 mg L⁻¹^[75] of nanoceria. Based on ICP studies, Ce-doped PGs did not reach 10 mg L⁻¹ in the current study. Another investigation on the influence of cerium oxide on proliferation, differentiation, and mineralization function of primary osteoblasts in vitro showed no toxicity for concentrations of 10⁻⁴ mol L⁻¹ (equal to 14 mg L⁻¹) of Ce³⁺.^[43] However, all previous studies were performed on cerium oxide nanoparticles, which have particular shape properties (roughness, sharp edges, and so on) and nanosize attributes potential to affect cell behavior.^[42,76,77] Several different in vitro studies have been conducted to investigate safe dose levels for gallium, due to the growing interest of gallium-based cancer therapies.^[78] Chandler et al. showed no cytotoxicity on L929 mouse fibroblasts at up to 1 mmol L⁻¹ (70 mg L⁻¹) of Ga³⁺.^[79]

3.7. Cell Behavior of ST-2 Cells in Indirect Contact with PGs

3.7.1. WST-8 Assay

WST-8 tests demonstrated the viability of ST-2 cells after 2 days of incubation with PG eluates (**Figure 9**). The best biological properties have been observed for 45P samples. The cell viability decreases with increase in gallium content (i.e., 7Ga shows 34% viable cells after 48 h) and increases with a rise of cerium content. These results, in combination with light microscope images of cell morphology (**Figure 10**), enable an evaluation of the relative cytotoxicity of the doped PGs studied. The highest value of cell viability (145%, positive control = 100%) was measured for 1 vol/wt% 45P, which is in agreement with literature.^[7,80] PGs of corresponding

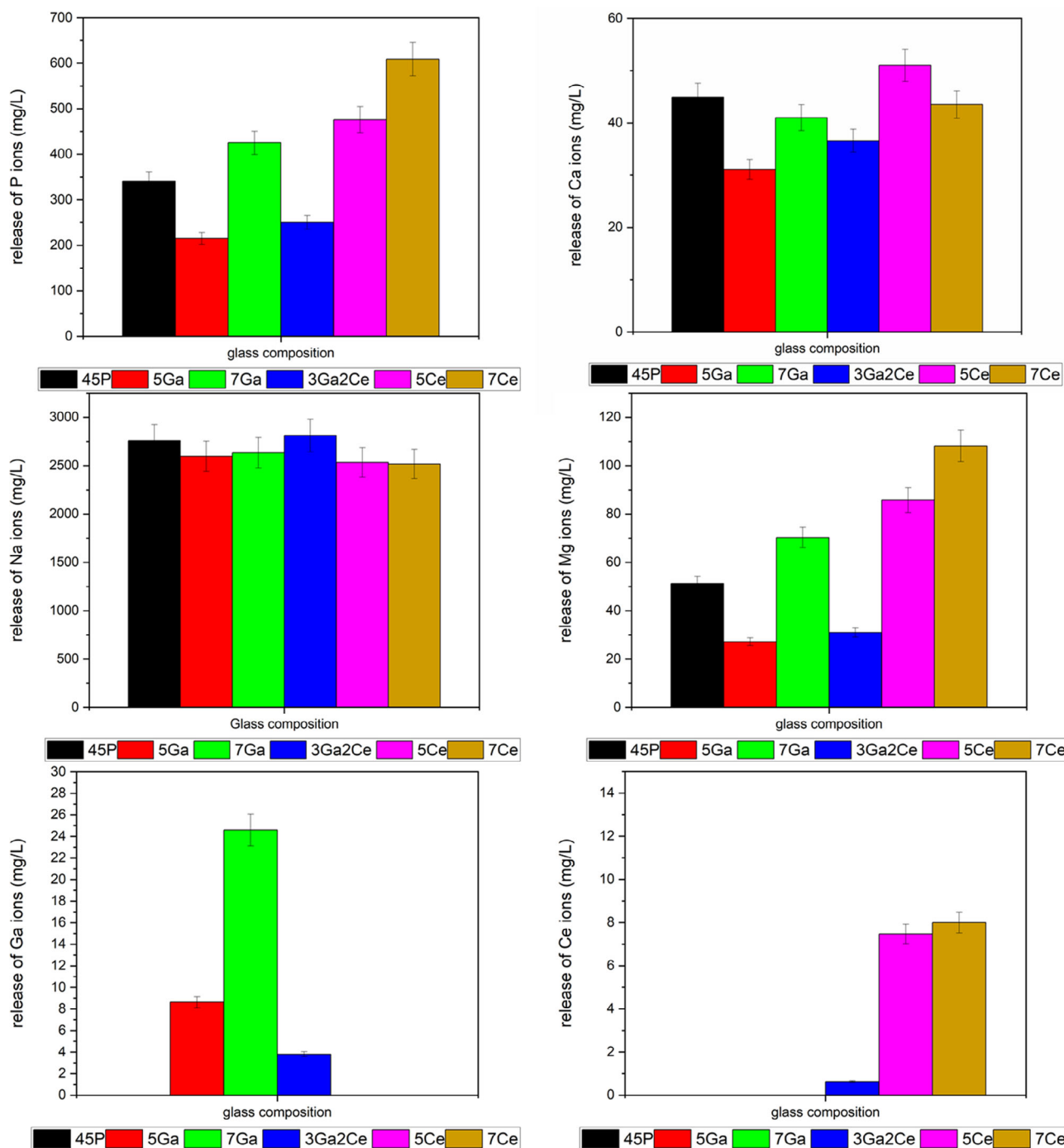


Figure 8. Ion release from PG after 24 h incubation in CCM.

composition have been shown to be suitable for both hard and soft tissue regeneration. Moreover, high contents of calcium^[7] and magnesium^[54] have been reported to improve cell adhesion of primary-derived human osteoblasts (HOB), and are nontoxic for MG63 and human ovarian fibroblast (HOF). Studies on glasses doped with 0, 10, 20, 30 mol% of MgO have shown no cytotoxicity for primary-derived HOBs^[54] with an increase in Mg content.

3.7.2. H&E Staining

Images of the cells on the well plate surface (1%) correspond to the results obtained from the WST-8 tests (Figure 10). Positive control samples were fully covered, and the cells were well spread, which suggest good attachment. Samples in the presence of 5Ce and 7Ga were poorly covered, cells were spread, but the number was significantly lower than for 5Ga, 3Ga2Ce, and 7Ce

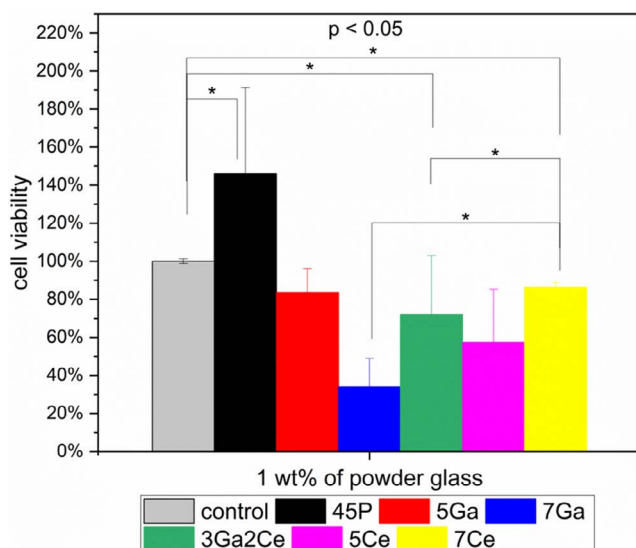


Figure 9. Cell viability of doped PG by the indirect contact method with ST-2 cells. Results are presented as a percentage of positive control (100%).

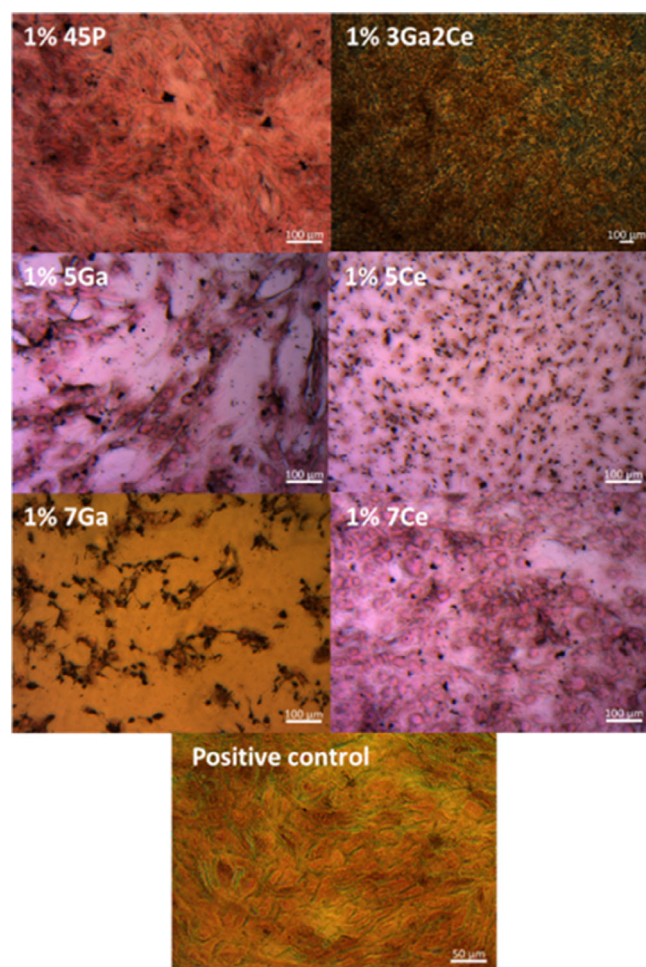


Figure 10. Light microscope images of ST-2 cells treated with the supernatant (1 wt/vol%) of PG (45P, 5Ga, 7Ga, 3Ga2Ce, 5Ce, 7Ce) after 48 h of incubation.

samples. The low cell response of 7Ga material may be caused by higher Ga^{3+} release combined with relatively low pH. Cells in contact with 1 wt/vol% of 7Ce glass were spread and formed a regular cell layer.

WST-8 results for cells exposed to 1 wt/vol% supernatant indicate that an increase in gallium content to 7 mol% decreases cell viability to 34%. This result could be attributed to high gallium release from the glass into the CCM as for glasses containing 5 mol% Ga, the measured cell viability was significantly higher at 83%. The ICP results revealed a high release of Ga ions: 24.6 and 8.63 mg L^{-1} after 24 h from 7Ga and 5Ga, respectively. Light microscopy images corresponding to the WST-8 results showed a decreased number of cells when incubated by indirect contact with glass 7Ga. The results are in agreement with the literature, where it has been shown that cytocompatibility decreased with increasing gallium content.^[34] Studies have been published claiming that 1 mol% Ga in mesoporous bioactive glass better supports the viability of human dermal fibroblasts compared with undoped and 2 or 3 mol% Ga glasses.^[81] In contrast, studies on bioactive glass doped with gallium showed an improvement in MC3T3-E1 cell viability compared with undoped glasses in systems doped with 5 and 7 mol% Ga.^[34] Gallium ions did not induce cell toxicity on fibroblasts,^[79] and the presence of Ga in mesoporous bioactive glass (1 mol%) was shown to improve the thrombus formation when in contact with blood compared with undoped glasses, whereas 3 mol% Ga decreased it.^[81] This result is in agreement with other studies showing that when enhancing antimicrobial properties, the biocompatibility is compromised.^[34]

Interestingly, an increase in cerium oxide content in PG tends to increase cell viability (57% and 86% viable cells for 5Ce and 7Ce, respectively). This correlates with higher confluency as confirmed by light microscope images. The confluency of ST-2 cells is higher when exposed to 1 wt/vol% supernatant of 7Ce than 5Ce, with cells showing better spreading and cell morphology. CeO_2 has been reported to show good cytocompatibility, antioxidant properties,^[75] and increased vascular endothelial growth factor production.^[42] In addition, Ce improves wound healing^[31] by supporting fibroblasts, keratinocytes, and vascular endothelial cells in a mouse wound model^[42] or enhancing leukocyte infiltration into wound tissue during the first 5 days of injury.^[42] Research of bioactive glasses doped with cerium has focused mainly on their antibacterial properties; however, CeO_2 -doped mica glass ceramics have been shown to stimulate osteoblast activity, improve cell viability, and increase alkaline phosphatase activity.^[82]

In our study, the viability of cells exposed to supernatant containing 1 wt/vol% of 3Ga2Ce (72%) PG sample was lower than that found in 5Ga (83%) or 7Ce (86%) samples. Such a system thus represents a suitable compromise between cytocompatibility and antibacterial properties.

3.8. Antibacterial Evaluation

Using the direct contact test method, all doped glasses showed antibacterial effect against both gram-positive and gram-negative bacteria over a period of 48 h compared with the control (Figure 11). The effectiveness was higher for gram-positive

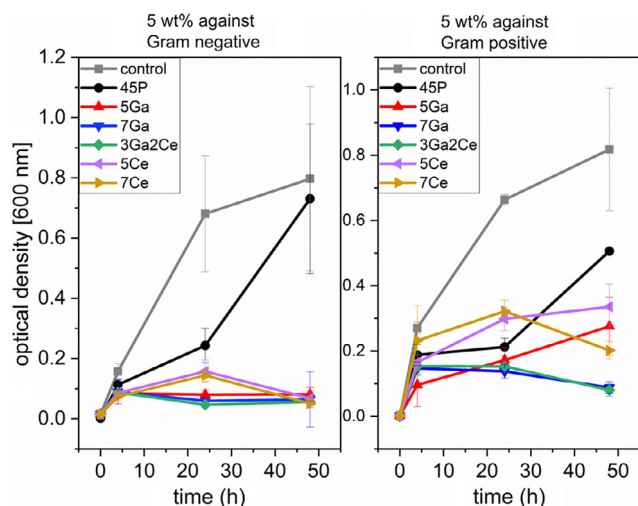


Figure 11. Antibacterial properties determined by OD measurement of doped PG against gram-positive and gram-negative bacteria.

species, and a decrease in OD was observed after only 4 h for some samples. However, a significant decrease in OD occurs after the first 24 h. The strongest antibacterial behavior is shown for 3Ga2Ce glass and for glasses doped with gallium (7Ga and 5Ga). The OD measured for those samples, which remained constant with time, suggests that bacterial growth had stopped. The result can be interpreted as an inhibitory effect of gallium and cerium on bacteria growth.

The antibacterial effects of gallium against *P. aeruginosa*, *S. aureus*, and *E. coli* have been reported.^[14,34] The highest antibacterial effect has been measured for glasses with relatively low gallium content (1–3 mol%). Moreover, the antibacterial effect does not always increase with increasing gallium content, as reported in the literature.^[14] Antibacterial properties of gallium are due to its similarity to Fe ions, an effect known as Trojan Horse strategy.^[14] In contrast, cerium oxide also showed an antibacterial effect but it was less effective than gallium ions. This result could be explained by a too low concentration of cerium oxide (5 and 7 mol%). However, it has been reported that 5 and 10 mol% of CeO₂ in silica fibers prevent the growth of *E. coli*.^[33] Moreover, gallium ions have been reported to be more effective against *S. aureus* than *E. coli* for Ga-MG, and the antibacterial effect has been shown to increase with increasing Ga content (1 mol% Ga, 2 mol% Ga, or 3 mol% Ga).^[81] Another reason why Ce appears to be less effective than Ga as an antibacterial ion might lie in its mechanism of action. Due to low availability of iron, bacteria develop ways of increasing uptake efficiency, and it is reasonable to assume the same route encourages gallium incorporation.^[30] Cerium has been proven to exhibit good antibacterial properties against *E. coli* and *S. aureus* by attacking the cell membrane.^[32] Studies on cerium nanoparticles have shown that antibacterial properties are concentration-dependent,^[76] which is in agreement with the results presented here, as the release of ions from CCM Ce⁴⁺ was lower than the release of Ga³⁺ (after 24 h). Summarizing, the results suggest an inhibitory effect of cerium- and gallium-doped PGs and demonstrate the suitability of the novel Ga/Ce containing PG for antibacterial applications.

Table 4. Summary and comparison of the key properties of novel PGs doped with gallium oxide and cerium oxide.

Glass composition	Degradation rate	pH	Cytocompatibility	Antibacterial properties
45P	–	++	++	–
5Ga	++	+	+	+
7Ga	++	–	–	++
3Ga2Ce	++	+	+	++
5Ce	+	+	–	+
7Ce	+	–	+	+

The key properties of all glass composition investigated are collected and compared in Table 4, which enables a rapid assessment of the positive and negative effects determined by the experimental results. It is apparent that by incorporating both Ga and Ce, a strong antibacterial response and good cytocompatibility were achieved.

4. Conclusions

The growing medical problem of bacteria resistance requires new approaches, prompting the development of antibiotic-free biomaterials with antibacterial capability. Novel gallium- and cerium-doped PGs with tunable solubility and antibacterial properties against *E. coli* and *S. carnosus* were investigated in this study. XRD analysis confirmed the amorphous character of the glasses. PG showed cytocompatible properties with up to 80% of viable ST-2 cells after 2 days of incubation. The high gallium levels in PG (up to 7 mol%) caused a high release of Ga³⁺ ions, which was proven to be toxic for cells (only 34% of viable cells remained after 2 days for PG with 7% Ga). Moreover, the addition of cerium and gallium ions influenced other properties of PG such as dissolution rate and pH. Changes in glass structure are proposed as a mechanism for these changes. Glasses doped with Ga provided a high antibacterial effect but became toxic for cells when the Ga content increased. Glasses doped with cerium oxide stopped (Gram-negative) or inhibited (Gram-positive) the growth of bacteria and showed good cytocompatibility, especially glasses containing 7 mol% of CeO₂. The current results indicate that PGs incorporating 7 mol% of cerium oxide are highly promising for medical applications. Another promising candidate is the glass with dual Ga and Ca doping (3Ga2Ce), which is similar to glass 7Ga in that it shows strong antibacterial properties for both Gram-negative and Gram-positive bacteria, but also exhibited cytocompatibility. The results thus proved that codoping can result in a PG which exhibits an effective antibacterial effect without being harmful to mammalian cells.

Acknowledgements

This research was conducted in the framework of HyMedPoly network, which received funding from the European Union's Horizon 2020 research and innovation program under the Marie Skłodowska-Curie grant agreement no. 643050.

Conflict of Interest

The authors declare no conflict of interest.

Keywords

antibacterial properties, cerium, gallium, ion release, medical applications, phosphate glasses

Received: December 27, 2019

Revised: February 6, 2020

Published online:

- [1] I. Ahmed, M. Lewis, I. Olsen, J. C. Knowles, *Biomaterials* **2004**, 25, 491.
- [2] R. Oueslati Omrani, A. Kaoutar, A. El Jazouli, S. Krimi, I. Khattech, M. Jemal, J. J. Videau, M. Couzi, *J. Alloys Compd.* **2015**, 632, 766.
- [3] D. Carta, J. C. Knowles, M. E. Smith, R. J. Newport, *J. Non-Cryst. Solids* **2007**, 353, 1141.
- [4] A. S. Monem, H. A. El Batal, E. M. A. Khalil, M. A. Azooz, Y. M. Hamdy, *J. Mater. Sci. Mater. Med.* **2008**, 19, 1097.
- [5] K. L. Skelton, J. V. Glenn, S. A. Clarke, G. Georgiou, S. P. Valappil, J. C. Knowles, S. N. Nazhat, G. R. Jordan, *Acta Biomater.* **2007**, 3, 563.
- [6] J. E. Gough, P. Christian, C. A. Scotchford, C. D. Rudd, I. A. Jones, *J. Biomed. Mater. Res.* **2002**, 59, 481.
- [7] M. Bitar, V. Salih, V. Mudera, J. C. Knowles, M. P. Lewis, *Biomaterials* **2004**, 25, 2283.
- [8] V. Salih, K. Franks, M. James, G. W. Hastings, J. C. Knowles, I. Olsen, *J. Mater. Sci. Mater. Med.* **2000**, 11, 615.
- [9] C. Zhu, I. Ahmed, A. Parsons, K. Z. Hossain, C. Rudd, J. Liu, X. Liu, *J. Non-Cryst. Solids* **2017**, 457, 77.
- [10] S. P. Valappil, M. Coombes, L. Wright, G. J. Owens, R. J. M. Lynch, C. K. Hope, S. M. Higham, *Acta Biomater.* **2012**, 8, 1957.
- [11] S. P. Valappil, J. C. Knowles, M. Wilson, *Appl. Environ. Microbiol.* **2008**, 74, 5228.
- [12] R. Ciceo Lucacel, A. O. Hulpus, V. Simon, I. Ardelean, *J. Non-Cryst. Solids* **2009**, 355, 425.
- [13] S. P. Valappil, D. Ready, E. A. Abou Neel, D. M. Pickup, L. A. O'Dell, W. Chrzanowski, J. Pratten, R. J. Newport, M. E. Smith, M. Wilson, J. C. Knowles, *Acta Biomater.* **2009**, 5, 1198.
- [14] S. P. Valappil, D. Ready, E. A. Abou Neel, D. M. Pickup, W. Chrzanowski, L. A. O'Dell, R. J. Newport, M. E. Smith, M. Wilson, J. C. Knowles, *Adv. Funct. Mater.* **2008**, 18, 732.
- [15] A. M. Mulligan, M. Wilson, J. C. Knowles, *Biomaterials* **2003**, 24, 1797.
- [16] E. A. Abou Neel, I. Ahmed, J. Pratten, S. N. Nazhat, J. C. Knowles, *Biomaterials* **2005**, 26, 2247.
- [17] E. A. Abou Neel, I. Ahmed, J. J. Blaker, A. Bismarck, A. R. Boccaccini, M. P. Lewis, S. N. Nazhat, J. C. Knowles, *Acta Biomater.* **2005**, 1, 553.
- [18] C. Vitale-Brovarone, G. Novajra, J. Lousteau, D. Milanese, S. Raimondo, M. Fornaro, *Acta Biomater.* **2012**, 8, 1125.
- [19] Y.-P. Kim, G.-S. Lee, J.-W. Kim, M. S. Kim, H.-S. Ahn, J.-Y. Lim, H.-W. Kim, Y.-J. Son, J. C. Knowles, *J. Tissue Eng. Regen. Med.* **2015**, 9, 236.
- [20] E. A. Abou Neel, V. Salih, J. C. Knowles, in *Comprehensive Biomaterials*, Elsevier **2011**, pp.285–297.
- [21] S. Lee, H. Maeda, A. Obata, K. Ueda, T. Narushima, T. Kasuga, *J. Non-Cryst. Solids* **2016**, 438, 18.
- [22] E. A. Abou Neel, W. Chrzanowski, D. M. Pickup, *J. R. Soc. Interface* **2009**, 6, 435.
- [23] U. Hoppe, G. Walter, R. Kranold, D. Stachel, A. Barz, *J. Non-Cryst. Solids* **1995**, 192193, 28.
- [24] R. L. Prabhakar, S. Brocchini, J. C. Knowles, *Biomaterials* **2005**, 26, 2209.
- [25] A. J. Alanis, *Arch. Med. Res.* **2005**, 36, 697.
- [26] K. N. Wilde, P. A. H. Nguyen, D. G. Whitten, H. E. Canavan, *Biointerphases* **2017**, 12, 02C403.
- [27] D. M. Pickup, S. P. Valappil, R. M. Moss, H. L. Twyman, P. Guerry, M. E. Smith, M. Wilson, J. C. Knowles, R. J. Newport, *J. Mater. Sci.* **2009**, 44, 1858.
- [28] M. Saugo, L. I. Brugnoli, D. O. Flamini, S. B. Saidman, *Mater. Sci. Eng. C* **2018**, 86, 62.
- [29] L. C. S. Antunes, F. Imperi, F. Minandri, P. Visca, *Antimicrob. Agents Chemother.* **2012**, 56, 5961.
- [30] F. Minandri, C. Bonchi, E. Frangipani, F. Imperi, P. Visca, *Future Microbiol.* **2014**, 9, 379.
- [31] W. W. Monofo, V. H. Ayvazian, A. M. Skinner, *Burns* **1958**, 3, 104.
- [32] X. Cai, G. J. Dai, S. Z. Tan, Y. Ouyang, Y. S. Ouyang, Q. S. Shi, *Mater. Lett.* **2012**, 67, 199.
- [33] Y. F. Goh, A. Z. Alshemary, M. Akram, M. R. Abdul Kadir, R. Hussain, *Ceram. Int.* **2014**, 40, 729.
- [34] A. M. Deliormanli, *Ceram. Int.* **2015**, 42, 897.
- [35] Y. Kaneko, M. Thoendel, O. Olakanmi, B. E. Britigan, P. K. Singh, *J. Clin. Invest.* **2007**, 117, 877.
- [36] P. Coltery, B. Keppler, C. Madoulet, B. Desoize, *Crit. Rev. Oncol. Hematol.* **2002**, 42, 283.
- [37] L. R. Bernstein, *Pharmacol. Rev.* **1998**, 50, 665.
- [38] S. Kaya, M. Cresswell, A. R. Boccaccini, *Mater. Sci. Eng. C* **2018**, 83, 99.
- [39] S. Pourshahrestani, E. Zeimaran, N. A. Kadri, N. Gargiulo, S. Samuel, S. V. Naveen, T. Kamarul, M. R. Towler, *J. Mater. Chem. B* **2016**, 4, 71.
- [40] S. Sanchez-Salcedo, G. Malavasi, A. J. Salinas, G. Lusvardi, L. Rigamonti, L. Menabue, M. Vallet-Regi, *Materials* **2018**, 11, 1.
- [41] N. Gómez-Cerezo, E. Verron, V. Montouillout, F. Fayon, P. Lagadec, J. M. Boulter, B. Bujoli, D. Arcos, M. Vallet-Regi, *Acta Biomater.* **2018**, 76, 333.
- [42] S. Chigurupati, M. R. Mughal, E. Okun, S. Das, A. Kumar, M. McCaffery, S. Seal, M. P. Mattson, *Biomaterials* **2013**, 34, 2194.
- [43] G. Zhou, G. Gu, Y. Li, Q. Zhang, W. Wang, S. Wang, J. Zhang, *Biol. Trace Elem. Res.* **2013**, 153, 411.
- [44] L. M. Placek, T. J. Keenan, A. Coughlan, A. W. Wren, *Biomed. Glasses* **2018**, 4, 32.
- [45] Y. M. Lai, X. F. Liang, S. Y. Yang, J. X. Wang, L. H. Cao, B. Dai, *J. Mol. Struct.* **2011**, 992, 84.
- [46] P. I. Paulose, G. Jose, V. Thomas, N. V. Unnikrishnan, M. K. R. Warrier, *J. Phys. Chem. Solids* **2003**, 64, 841.
- [47] B. W. Stuart, C. A. Grant, G. E. Stan, A. C. Popa, J. J. Titman, D. M. Grant, *J. Mech. Behav. Biomed. Mater.* **2018**, 82, 371.
- [48] U. Hoppe, D. Ilieva, J. Neufelnd, *Z. Naturforsch.* **2002**, 57, 709.
- [49] A. Belkibir, J. Rocha, A. P. Esculcas, P. Berthet, S. Poisson, B. Gilbert, Z. Gabelica, G. Llabres, F. Wijzen, A. Rulmont, *Spectrochim. Acta Part A* **2000**, 56, 423.
- [50] P. Balasubramanian, R. Detsch, L. Esteban-Tejeda, A. Grünwald, J. S. Moya, A. R. Boccaccini, *Biomed. Glasses* **2017**, 3, 104.
- [51] Dojindo Molecular Technologies, https://www.dojindo.com/TechnicalManual/Manual_CK04.pdf (accessed: February 2019).
- [52] Washington University School of Medicine, Hematoxylin & Eosin Stain Protocol, <https://neuromuscular.wustl.edu/pathol/histol/HE.pdf> (accessed: February 2019).
- [53] L. Gritsch, C. Lovell, W. H. Goldmann, A. R. Boccaccini, *J. Mater. Sci. Mater. Med.* **2018**, 29, 2.
- [54] I. Ahmed, A. Parsons, A. Jones, G. Walker, C. Scotchford, C. Rudd, *J. Biomater. Appl.* **2010**, 24, 555.
- [55] D. Carta, D. M. Pickup, J. C. Knowles, I. Ahmed, M. E. Smith, R. J. Newport, *J. Non-Cryst. Solids* **2007**, 353, 1759.
- [56] Y. Lai, X. Liang, S. Yang, P. Liu, Y. Zeng, C. Hu, *J. Alloys Compd.* **2014**, 617, 597.

- [57] A. K. Yadav, P. Singh, *RSC Adv.* **2015**, 5, 67583.
- [58] A. Mishra, J. Rocherullé, J. Massera, *J. Biomed. Glasses* **2016**, 2, 1.
- [59] W. A. Pisarski, L. Žur, T. Goryczka, M. Sołtys, J. Pisarska, *J. Alloys Compd.* **2014**, 587, 90.
- [60] L. Muñoz-Senovilla, F. Muñoz, G. Tricot, I. Ahmed, A. J. Parsons, *J. Mater. Sci.* **2017**, 52, 9166.
- [61] J. J. Hudgens, R. K. Brow, D. R. Tallant, S. W. Martin, *J. Non-Cryst. Solids* **1998**, 223, 21.
- [62] B. C. Bunker, G. W. Arnold, J. A. Wilder, *J. Non-Cryst. Solids* **1984**, 64, 291.
- [63] I. Ahmed, M. Lewis, I. Olsen, J. C. Knowles, *Biomaterials* **2004**, 25, 501.
- [64] A. Belkébir, J. Rocha, A. P. Esculcas, P. Berthet, B. Gilbert, Z. Gabelica, G. Llabres, F. Wijzen, A. Rulmont, *Spectrochim. Acta Part A* **2000**, 56, 435.
- [65] A. M. Deliormanlı, *J. Mater. Sci. Mater. Med.* **2015**, 26, 1.
- [66] J. Ren, H. Eckert, *J. Phys. Chem. C* **2014**, 118, 15386.
- [67] J. Belcher, J. L. Rygel, L. Kokou, C. G. Pantano, Y. Chen, R. Woodman, J. Du, *J. Am. Ceram. Soc.* **2011**, 94, 2393.
- [68] N. Wantana, E. Kaewnuam, N. Chanthima, S. Kaewjaeng, H. J. Kim, J. Kaewkhao, M. A. Marzouk, H. A. ElBatal, Y. M. Hamdy, F. M. Ezz-Eldin, S. H. Morgan, R. H. Magruder, E. Silberman, H. Shinozaki, S. Nakashima, S. Takahashi, A. Hanada, Y. Yamamoto, J.-M. Cha, J.-H. Kim, B.-K. Ryu, *J. Non-Cryst. Solids* **2018**, 44, S172.
- [69] H. Shinozaki, S. Nakashima, S. Takahashi, A. Hanada, Y. Yamamoto, *J. Non-Cryst. Solids* **2013**, 378, 55.
- [70] F. Döhler, A. Mandlule, L. van Wüllen, M. Friedrich, D. S. Brauer, *J. Mater. Chem. B* **2015**, 3, 1125.
- [71] N. Sharmin, M. S. Hasan, A. J. Parsons, C. D. Rudd, I. Ahmed, *J. Mech. Behav. Biomed. Mater.* **2016**, 59, 41.
- [72] U. Hansen, A. F. Thünemann, *Langmuir* **2015**, 31, 6842.
- [73] M. Arora, *Mater. Methods* **2013**, 3, 175.
- [74] J. C. Wataha, R. G. Craig, C. T. Hanks, *J. Dent. Res.* **1991**, 70, 1014.
- [75] D. Schubert, R. Dargusch, J. Raitano, S. W. Chan, *Biochem. Biophys. Res. Commun.* **2006**, 342, 86.
- [76] I. Albuquerque, P. Farias, C. Christiano, F. C. Sampaio, *Biomed. Res. Int.* **2018**, 2018, 14.
- [77] P. Sobhanachalam, V. Ravi Kumar, N. Venkatramaiah, Y. Gandhi, N. Veeraiah, *J. Non-Cryst. Solids* **2018**, 498, 422.
- [78] C. R. Chitambar, *Int. J. Environ. Res. Public Health* **2010**, 7, 2337.
- [79] J. E. Chandler, H. H. Messer, G. Ellender, *J. Dent. Res.* **1994**, 73, 1554.
- [80] M. Bitar, J. C. Knowles, M. P. Lewis, V. Salih, *J. Mater. Sci. Mater. Med.* **2005**, 16, 1131.
- [81] S. Pourshahrestani, E. Zeimaran, N. Adib Kadri, N. Gargiulo, S. Samuel, S. V. Naveen, T. Kamarul, M. R. Towler, *J. Mater. Chem. B* **2016**, 4, 71.
- [82] I. Akin, G. Goller, *J. Ceram. Soc. Jpn.* **2009**, 117, 787.